PHYSICAL REVIEW B **78**, 220501(R) (2008)

High-energy spin excitations in $BaFe_2As_2$ observed by inelastic neutron scattering

R. A. Ewings,[1] T. G. Perring,[1] R. I. Bewley,[1] T. Guidi,[1] M. J. Pitcher,[2] D. R. Parker,[2] S. J. Clarke,[2] and A. T. Boothroyd[3,*]
[1]*ISIS Facility, Rutherford Appleton Laboratory, Chilton, Didcot OX11 0QX, United Kingdom*
[2]*Department of Chemistry, Inorganic Chemistry Laboratory, Oxford University, Oxford OX1 3QR, United Kingdom*
[3]*Department of Physics, Clarendon Laboratory, Oxford University, Oxford OX1 3PU, United Kingdom*
(Received 9 October 2008; published 2 December 2008)

We report neutron-scattering measurements of cooperative spin excitations in antiferromagnetically ordered $BaFe_2As_2$, the parent phase of an iron pnictide superconductor. The data extend up to ~100 meV and show that the spin excitation spectrum is sharp and highly dispersive. By fitting the spectrum to a linear spin-wave model we estimate the magnon bandwidth to be in the region of 0.17 eV. The large characteristic spin-fluctuation energy suggests that magnetism could play a role in the formation of the superconducting state.

DOI: 10.1103/PhysRevB.78.220501 PACS number(s): 74.25.Ha, 74.70.Dd, 75.30.Ds, 78.70.Nx

One of the greatest challenges presented by the recently discovered iron pnictide superconductors[1] is to identify the electron pairing interaction which permits the formation of a superconducting condensate. In conventional superconductors this interaction is provided by the exchange of a phonon. For the iron pnictides, however, theoretical calculations[2,3] indicate that the electron-phonon coupling is too weak to account for the observed high critical temperatures. Attention has therefore turned to other types of bosonic excitations which could mediate the pairing interaction.

One such candidate is spin fluctuations.[4] In common with the layered cuprates, superconductivity in the pnictides is found in close proximity to parent phases which exhibit long-range antiferromagnetic (AFM) order.[5,6] However, unlike the cuprates, whose magnetic properties are governed by strong superexchange interactions between localized spin-$\frac{1}{2}$ moments in a single Cu $3d_{x^2-y^2}$ orbital, magnetism in the pnictides is more itinerant in character and derives from multiple d orbitals. It may also involve a degree of frustration. Studies of the spin dynamics in the magnetically ordered parent phases of unconventional superconductors such as the cuprates and iron pnictides are important to establish the prominent characteristics and energy scales of the spin fluctuations and to provide a clean reference against which superconductivity-induced changes can be identified.

Recent low-energy neutron-scattering measurements on single crystals of $SrFe_2As_2$ (Ref. 7) and $CaFe_2As_2$ (Ref. 8) revealed spin-wave excitations up to ~25 meV with a spin gap of 6–7 meV. A large in-plane spin-wave velocity was inferred, suggesting that the spin excitation spectrum could extend to much higher energies. Here we report neutron-scattering data on polycrystalline $BaFe_2As_2$ which reveal spin-wave excitations up to 100 meV, a significantly higher energy than previously reached. This enables us to use a spin-wave model to place tight constraints on the magnon bandwidth which we find to be in the region of 0.17 eV, not much less than that in the cuprates. Such a high characteristic energy suggests that spin fluctuations are a serious candidate to mediate high-temperature superconductivity in the iron pnictides.

The parent phase $BaFe_2As_2$ becomes superconducting on doping with holes[9] or on application of pressure.[10] At T_s = 140 K, $BaFe_2As_2$ undergoes a structural transition from tetragonal to orthorhombic and simultaneously develops three-dimensional long-range antiferromagnetic order.[11–13] On cooling through T_s, the space group changes from $I4/mmm$ (lattice parameters a=3.96 Å and c=13.0 Å) to $Fmmm$ (lattice parameters a=5.61 Å, b=5.57 Å, and c =12.9 Å). The magnetic structure of $BaFe_2As_2$, shown in Fig. 1, is a collinear antiferromagnet with propagation vector $\mathbf{Q}_{AF}=(1,0,1)$. The ordered moments on the Fe atoms have an approximate magnitude of $0.9\mu_B$ and point along the orthorhombic a axis.

Polycrystalline $BaFe_2As_2$ was prepared by reacting stoichiometric amounts of the elements in a tantalum ampoule sealed under argon (800 °C for 2 days, then 900 °C for 2 days after regrinding). Phase purity was confirmed using x-ray powder diffraction. The neutron-scattering experiments were performed on the MERLIN chopper spectrometer at the ISIS Facility.[14] Approximately 8 g of the $BaFe_2As_2$ powder was sealed inside a cylindrical aluminum can and mounted in a top-loading closed-cycle refrigerator. Spectra were recorded at a temperature of 7 K with four different neutron incident energies: E_i=25, 50, 200, and 400 meV. The scattering from a standard vanadium sample was used to normalize the spectra and to place them on an absolute intensity scale with units mb sr^{-1} meV^{-1} f.u.$^{-1}$, where 1 mb $=10^{-31}$ m^2 and f.u. stands for "formula unit" (of $BaFe_2As_2$). The spectra were azimuthally averaged and transformed onto

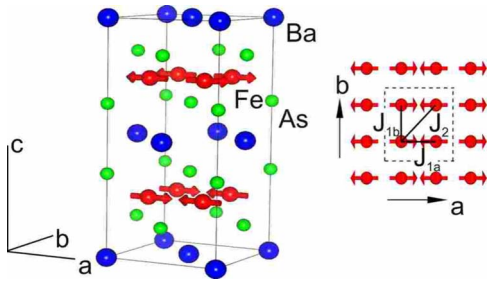

FIG. 1. (Color online) Crystal and magnetic structure of $BaFe_2As_2$. On the left is the crystal structure with the conventional unit cell for the low-temperature orthorhombic $Fmmm$ structure. The three-dimensional AFM ordering of Fe spins is indicated. On the right is a single layer of Fe spins showing the in-plane AFM order and the nearest- and next-nearest-neighbor exchange interactions.

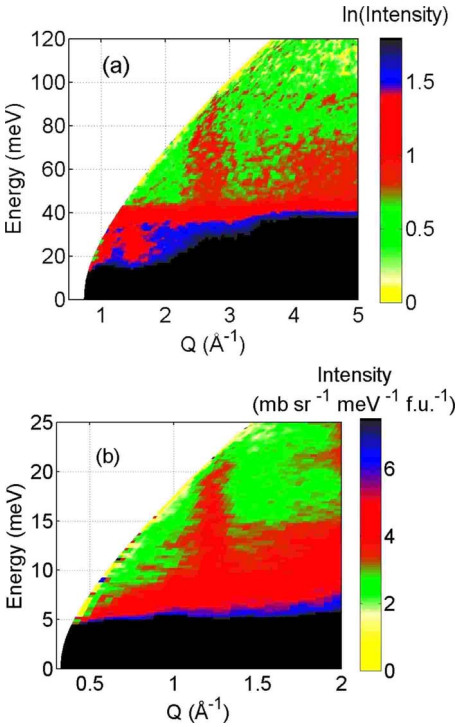

FIG. 2. (Color online) Neutron scattering spectra of $BaFe_2As_2$. The data were recorded at a temperature of 7 K with incident neutron energies of (a) 200 meV (logarithmic scale) and (b) 50 meV. The pillars of scattering centered near $Q=1.2$ Å^{-1} and $Q=2.6$ Å^{-1} are caused by highly dispersive collective excitations associated with the antiferromagnetically ordered Fe spins (see Fig. 1). (b) is a higher resolution image showing the magnetic signal emerging from $Q=1.2$ Å^{-1}.

a (Q, energy) grid, where $Q=|\mathbf{Q}|$ is the magnitude of the neutron-scattering vector. The presented intensity is the partial differential cross section $d^2\sigma/d\Omega dE_f$ multiplied by the factor k_i/k_f,[18] where k_i and k_f are the initial and final neutron wave vectors and E_f is the final neutron energy.

Figure 2(a) illustrates the general features of the data. At low energies there is strong diffuse scattering due to the elastic peak and scattering from phonons, the latter of which increases with Q. The phonon signal drops off sharply above 40 meV, which is the upper limit of the vibrational density of states.[15] Two distinct features stand out from the phonon signal. One is a narrow pillar of scattering at $Q=1.2$ Å^{-1} and the second is a plume of intensity centered on $Q=2.6$ Å^{-1}. The latter extends in energy to at least 90 meV where it disappears out of the accessible region of (Q, energy) space. The 1.2 Å^{-1} feature is followed to lower energies in Fig. 2(b), which was obtained with a higher resolution configuration.

The origin of the 1.2 and 2.6 Å^{-1} features is the cooperative spin-wave excitations (magnons) associated with the AFM zone centers $(1,0,l)$ and $(1,2,l)$. Since the structure is layered we expect only a weak variation in the inelastic scattering with l. The effect of powder averaging and resolution folding makes the two-dimensional (2D) magnon scattering appear at slightly higher Q than the 2D AFM wave vectors $Q_{(1,0)}=1.1$ Å^{-1} and $Q_{(1,2)}=2.5$ Å^{-1}, as observed in Fig. 2.

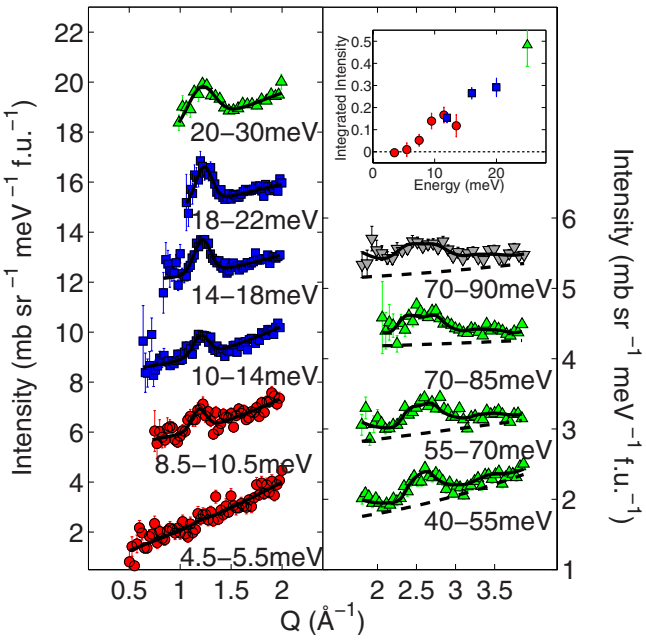

FIG. 3. (Color online) The left and right panels show a series of constant-energy cuts through the magnon signals at $Q=1.2$ Å^{-1} and $Q=2.6$ Å^{-1}, respectively. The data were averaged over the energy ranges indicated. Successive cuts are displaced vertically for clarity. The symbols represent different neutron incident energies: 25 meV (red circles), 50 meV (blue squares), 200 meV (green triangles), and 400 meV (gray inverted triangles). In the left panel the lines are fits to Gaussian peaks on a sloping background. In the right panel the lines are constant-energy cuts (averaged over the same energy ranges as the data) through the powder-averaged spin-wave spectrum calculated with parameters $SJ_2=2SJ_{1a}=2SJ_{1b}=35$ meV, $J_c=0$, $SK_{ab}=SK_c=0.042$ meV, and $S_{\text{eff}}=0.28$ (see Fig. 4). The inset shows the integrated intensities of the magnon scattering measured at $Q=1.2$ Å^{-1} as a function of energy.

Figure 3 shows examples of a series of cuts taken through the data at different energies. At the higher energies the signal is seen to broaden (right panel). This is due to dispersion of the spin waves. Below ~15 meV the magnetic signal decreases in intensity. We fitted the cuts taken through $Q=1.2$ Å^{-1} with a Gaussian line shape on a quadratic background and plot the integrated intensities of the fitted peaks at each energy in the inset of Fig. 3. The data show that the magnetic excitations are gapped, with no detectable signal below 5 meV. However, the gap is not sharp since a sharp gap would produce a stepwise increase in intensity at the gap energy with a resolution broadening of only 1–2 meV, unlike the more gradual increase seen in Fig. 3 (inset). The broadening of the step could be due to the dispersion in the c direction[7,8] and/or the existence of two or more gaps in the 5–15 meV range. Indeed, in orthorhombic symmetry two gaps are expected at $\mathbf{Q}_{\text{AF}}$ as a result of magnetic anisotropy which splits the spin waves into two nondegenerate branches with predominantly in-plane and out-of-plane characters.

We now compare our data with a linear spin-wave model for $BaFe_2As_2$ based on an effective Heisenberg spin Hamiltonian. The suitability of such a model is perhaps questionable in view of the itinerant character of the magnetism,[16] but at the very least it will provide an estimate of the scale of

the magnetic interactions. We calculated the spectrum using a similar method to that of Yao and Carlson[17] but extended the Hamiltonian to include terms that represent the single-ion anisotropy,

$$H = \sum_{\langle jk \rangle} J_{jk} \mathbf{S}_j \cdot \mathbf{S}_k + \sum_j \{K_c (S_z^2)_j + K_{ab}(S_y^2 - S_x^2)_j\}. \quad (1)$$

The first summation is over nearest-neighbor and next-nearest-neighbor pairs with each pair counted only once. The J_{jk} are exchange parameters as defined in Fig. 1 and K_{ab} and K_c are in-plane and out-of-plane anisotropy constants, respectively. Diagonalization of Eq. (1) leads to two nondegenerate branches with dispersion,

$$\hbar\omega_{1,2}(\mathbf{Q}) = \sqrt{A_\mathbf{Q}^2 - (C \pm D_\mathbf{Q})^2}, \quad (2)$$

where

$$A_\mathbf{Q} = 2S\left\{J_{1b}\left[\cos\left(\frac{\mathbf{Q}\cdot\mathbf{b}}{2}\right) - 1\right] + J_{1a} + 2J_2 + J_c\right\} + S(3K_{ab} + K_c),$$

$$C = S(K_{ab} - K_c),$$

$$D_\mathbf{Q} = 2S\left\{J_{1a}\cos\left(\frac{\mathbf{Q}\cdot\mathbf{a}}{2}\right) + 2J_2\cos\left(\frac{\mathbf{Q}\cdot\mathbf{a}}{2}\right)\cos\left(\frac{\mathbf{Q}\cdot\mathbf{b}}{2}\right) + J_c\cos(\mathbf{Q}\cdot\mathbf{c})\right\}. \quad (3)$$

The neutron-scattering cross section may be written as[18]

$$\frac{d^2\sigma}{d\Omega dE_f} = \frac{k_f}{k_i}\left(\frac{\gamma r_0}{2}\right)^2 g^2 f^2(Q)\exp(-2W) \times \sum_{\alpha\beta}(\delta_{\alpha\beta} - \hat{Q}_\alpha\hat{Q}_\beta)S^{\alpha\beta}(\mathbf{Q},\omega), \quad (4)$$

where $(\gamma r_0/2)^2 = 72.8$ mb, g is the g factor of iron, $f(Q)$ is the form factor of iron, $\exp(-2W)$ is the Debye-Waller factor which is close to unity at low temperatures, $\hat{Q}_\alpha$ is the α component of a unit vector in the direction of $\mathbf{Q}$, and $S^{\alpha\beta}(\mathbf{Q},\omega)$ is the response function describing $\alpha\beta$ spin correlations. Only the transverse correlations (yy and zz for $BaFe_2As_2$) contribute to the linear spin-wave cross section and the response functions (per $BaFe_2As_2$ f.u.) for magnon creation are given by

$$S^{yy}(\mathbf{Q},\omega) = S_{\text{eff}}\frac{A_\mathbf{Q} - C - D_\mathbf{Q}}{\hbar\omega_1(\mathbf{Q})}\{n(\omega)+1\}\delta[\omega - \omega_1(\mathbf{Q})],$$

$$S^{zz}(\mathbf{Q},\omega) = S_{\text{eff}}\frac{A_\mathbf{Q} + C - D_\mathbf{Q}}{\hbar\omega_2(\mathbf{Q})}\{n(\omega)+1\}\delta[\omega - \omega_2(\mathbf{Q})], \quad (5)$$

where S_{eff} is the effective spin and $n(\omega)$ is the boson occupation number. In linear spin-wave theory $S_{\text{eff}} = S$, but we keep S and S_{eff} distinct here because in the analysis they are obtained essentially independently (see below).

Because our data do not extend over the full spin-wave dispersion we were unable to determine J_{1a}, J_{1b}, and J_2 independently. However, several authors[19–22] have made predictions of effective Heisenberg exchange parameters from first-principles electronic structure calculations. In some cases[19–21] J_2 is predicted to exceed J_{1a} and J_{1b} by about a factor of 2, with J_{1a} and J_{1b} either both ferromagnetic or both AFM (providing J_{1a} and J_{1b} are the same sign the spectrum at low energies is not very sensitive to the sign[17]). Alternatively,[22] $J_{1a} \gg J_{1b}$ and $J_{1a} \simeq 2J_2$. Guided by these predictions we fixed the ratios of the exchange parameters to be either (i) $J_{1a} = J_{1b} = J_2/2$ or (ii) $J_{1a} = 2J_2 = -5J_{1b}$. Since we cannot resolve more than one gap in the data we set $K_{ab} = K_c$ so that the in-plane and out-of-plane gaps are the same, and we neglected the c-axis coupling, which is expected to be much smaller than the in-plane coupling. The g factor was set to 2.

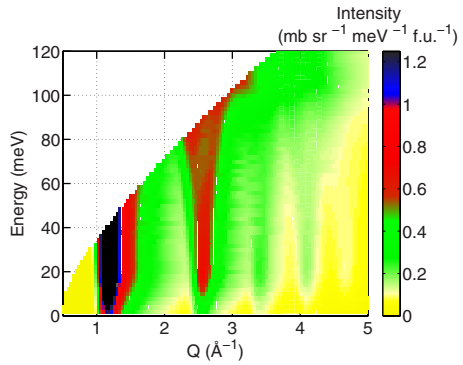

FIG. 4. (Color online) Simulation of the powder-averaged spin-wave spectrum of $BaFe_2As_2$. The simulation covers the same Q and energy range as the data in Fig. 2(a). The parameters used for the simulation are given in the caption to Fig. 3.

We computed the powder-averaged spin-wave spectrum convoluted with the instrumental resolution and fitted it to the experimental data near $Q = 2.6$ Å^{-1} allowing only SJ_2 and S_{eff} to vary. S_{eff} is essentially determined by the absolute intensity and SJ_2 by the dispersion. Data near $Q = 1.2$ Å^{-1} were excluded as the peak widths are dominated by instrument resolution and consequently are insensitive to SJ_2. We obtained equally good fits to the data with both sets of parameter ratios. The best-fit parameters are as follows: for case (i) $SJ_2 = 35 \pm 3$ meV and $S_{\text{eff}} = 0.28 \pm 0.04$ and for case (ii) $SJ_2 = 18 \pm 1$ meV and $S_{\text{eff}} = 0.54 \pm 0.05$. The highest resolution data reveal a gap of 7.7 ± 0.2 meV—Fig. 3 (inset)—which yields $SK_c = SK_{ab} = 0.042 \pm 0.004$ meV [case (i)] and 0.053 ± 0.005 meV [case (ii)]. For case (i) we tried different values of J_1/J_2, but the best-fit value of SJ_2 was relatively insensitive, varying from 33 meV ($J_1/J_2 = 0.25$) to 46 meV ($J_1/J_2 = 1$). Aside from the uncertainty in J_1/J_2, the major error in SJ_2 is the statistical error on the fit. The error in S_{eff} comes from estimates of the background and instrumental resolution.

Figure 4 shows the powder-averaged spin-wave spectrum calculated with the best-fit parameters for case (i) over the same range of Q and energy covered by the measurements in Fig. 2(a). The maximum spin-wave energy is ~175 meV for both parameter sets, well out of range of the present experiment. We note that the order of magnitude of the experimen-

tally determined exchange parameters is consistent with theoretical predictions[19–22] providing S is close to unity. The values of gS_{eff} [0.56 for case (i) and 1.08 for case (ii)] obtained from our analysis are comparable with the measured ordered moment in μ_B of 0.8–0.9.[12,13]

Our results show that spin fluctuations in the parent phase of the pnictides exist over a wide energy range extending up to ~175 meV, not much less than that found in the cuprate high-temperature superconductors. For high T_c it is natural to look for a pairing boson with a large characteristic energy. The data here show that spin fluctuations satisfy this requirement. However, if magnetism is to play a role in the superconducting state, then there must also be a coupling between spin fluctuations and the electrons involved in pairing. One piece of evidence for this is the recent observation of a resonant spin excitation in the superconducting state of $Ba_{0.6}K_{0.4}Fe_2As_2$.[23] More generally, the itinerant character of magnetism in the pnictides has been inferred from the nesting of electron and hole Fermi-surface pockets with nesting vector $\mathbf{Q}_{\mathrm{AF}}$ (Refs. 5 and 24–26) and by the observed effect of AFM order on the Fermi surface as revealed, for example, by optical spectroscopy,[5,27] angle-resolved photoemission spectroscopy,[28] and quantum oscillations.[29]

On the other hand, the dynamic magnetic response measured here does not show any obvious fingerprints of itinerant magnetism, such as damping due to a Stoner continuum. It will be interesting to follow the spin excitation spectrum to still higher energies where itinerant effects generally have the largest influence.

We thank I. I. Mazin for helpful comments. This work was supported by the Engineering and Physical Sciences Research Council of Great Britain.

*a.boothroyd@physics.ox.ac.uk

[1] Y. Kamihara, T. Watanabe, M. Hirano, and H. Hosono, J. Am. Chem. Soc. **130**, 3296 (2008).
[2] L. Boeri, O. V. Dolgov, and A. A. Golubov, Phys. Rev. Lett. **101**, 026403 (2008).
[3] K. Haule, J. H. Shim, and G. Kotliar, Phys. Rev. Lett. **100**, 226402 (2008).
[4] D. J. Singh and M.-H. Du, Phys. Rev. Lett. **100**, 237003 (2008).
[5] J. Dong, H. J. Zhang, G. Xu, Z. Li, G. Li, W. Z. Hu, D. Wu, G. F. Chen, X. Dai, J. L. Luo, Z. Fang, and N. L. Wang, Europhys. Lett. **83**, 27006 (2008).
[6] C. de la Cruz, Q. Huang, J. W. Lynn, J. Li, W. Ratcliff II, J. L. Zarestky, H. A. Mook, G. F. Chen, J. L. Luo, N. L. Wang, and P. Dai, Nature (London) **453**, 899 (2008).
[7] J. Zhao, D.-X. Yao, S. Li, T. Hong, Y. Chen, S. Chang, W. Ratcliff II, J. W. Lynn, H. A. Mook, G. F. Chen, J. L. Luo, N. L. Wang, E. W. Carlson, J. Hu, and P. Dai, Phys. Rev. Lett. **101**, 167203 (2008).
[8] R. J. McQueeney, S. O. Diallo, V. P. Antropov, G. D. Samolyuk, C. Broholm, N. Ni, S. Nandi, M. Yethiraj, J. L. Zarestky, J. J. Pulikkotil, A. Kreyssig, M. D. Lumsden, B. N. Harmon, P. C. Canfield, and A. I. Goldman, arXiv:0809.1410 (unpublished).
[9] M. Rotter, M. Tegel, and D. Johrendt, Phys. Rev. Lett. **101**, 107006 (2008).
[10] P. L. Alireza, J. Gillett, Y. T. Chris Ko, S. E. Sebastian, and G. G. Lonzarich, arXiv:0807.1896, J. Phys.: Condens. Matter (to be published).
[11] M. Rotter, M. Tegel, D. Johrendt, I. Schellenberg, W. Hermes, and R. Pöttgen, Phys. Rev. B **78**, 020503(R) (2008).
[12] Q. Huang, Y. Qiu, W. Bao, M. A. Green, J. W. Lynn, Y. C. Gasparovic, T. Wu, G. Wu, and X. H. Chen, arXiv:0806.2776 (unpublished).
[13] Y. Su, P. Link, A. Schneidewind, Th. Wolf, Y. Xiao, R. Mittal, M. Rotter, D. Johrendt, Th. Brueckel, and M. Loewenhaupt, arXiv:0807.1743 (unpublished).
[14] R. I. Bewley, R. S. Eccleston, K. A. McEwen, S. M. Hayden, M. T. Dove, S. M. Bennington, J. R. Treadgold, and R. L. S. Coleman, Physica B **385-386**, 1029 (2006).
[15] R. Mittal, Y. Su, S. Rols, T. Chatterji, S. L. Chaplot, H. Schober, M. Rotter, D. Johrendt, and Th. Brueckel, Phys. Rev. B **78**, 104514 (2008).
[16] I. I. Mazin, M. D. Johannes, L. Boeri, K. Koepernik, and D. J. Singh, arXiv:0806.1869 (unpublished).
[17] D. X. Yao and E. W. Carlson, Phys. Rev. B **78**, 052507 (2008).
[18] G. L. Squires, *Introduction to the Theory of Thermal Neutron Scattering* (Dover, New York, 1996).
[19] T. Yildirim, Phys. Rev. Lett. **101**, 057010 (2008).
[20] Q. Si and E. Abrahams, Phys. Rev. Lett. **101**, 076401 (2008).
[21] F. Ma, Z.-Y. Lu, and T. Xiang, arXiv:0804.3370 (unpublished).
[22] Z. P. Yin, S. Lebègue, M. J. Han, B. P. Neal, S. Y. Savrasov, and W. E. Pickett, Phys. Rev. Lett. **101**, 047001 (2008).
[23] A. D. Christianson, E. A. Goremychkin, R. Osborn, S. Rosenkranz, M. D. Lumsden, C. D. Malliakas, I. S. Todorov, H. Claus, D. Y. Chung, M. G. Kanatzidis, R. I. Bewley, and T. Guidi, arXiv:0807.3932 (unpublished).
[24] V. Cvetkovic and Z. Tesanovic, arXiv:0804.4678 (unpublished).
[25] F. Ma and Z.-Y. Lu, Phys. Rev. B **78**, 033111 (2008).
[26] K. Kuroki, S. Onari, R. Arita, H. Usui, Y. Tanaka, H. Kontani, and H. Aoki, Phys. Rev. Lett. **101**, 087004 (2008).
[27] W. Z. Hu, J. Dong, G. Li, Z. Li, P. Zheng, G. F. Chen, J. L. Luo, and N. L. Wang, arXiv:0806.2652 (unpublished).
[28] L. X. Yang, Y. Zhang, H. W. Ou, J. F. Zhao, D. W. Shen, B. Zhou, J. Wei, F. Chen, M. Xu, C. He, Y. Chen, Z. D. Wang, X. F. Wang, T. Wu, G. Wu, X. H. Chen, M. Arita, K. Shimada, M. Taniguchi, Z. Y. Lu, T. Xiang, and D. L. Feng, arXiv:0806.2627 (unpublished).
[29] S. E. Sebastian, J. Gillett, N. Harrison, C. H. Mielke, S. K. Goh, P. H. C. Lau, and G. G. Lonzarich, J. Phys.: Condens. Matter **20**, 422203 (2008).